

Fröhlich Polarons From 3D to 0D. Concepts and Recent Developments

J. T. DEVREESE

*Theoretische Fysica van de Vaste Stoffen, Universiteit Antwerpen
CDE, Universiteitsplein, 1, B-2610 Antwerpen, Belgium
and eiTT/COBRA interuniversitaire onderzoekschool, TU Eindhoven
NL-5600 MB Eindhoven, The Netherlands*

Summary. — An overview is presented of the fundamentals of continuum-polaron physics, which provide the basis of the analysis of polaron effects in ionic crystals and polar semiconductors. The present paper deals with “large”, or “continuum”, polarons, as described by the Fröhlich Hamiltonian. The emphasis is on the polaron optical absorption.

PACS 71.38.-k, 63.20.Kr, 71.38.Mx, 71.10.-w, 73.21.-b, 74.20.Mn

1. – The Polaron Concept

As is generally known, the polaron concept was introduced by Landau in 1933 [1]. Gradually a distinction was made between polarons in the continuum approximation where long-range electron-lattice interaction prevails (“Fröhlich” polarons) and polarons for which the short-range interaction is essential (Holstein, Holstein-Hubbard models). After a period of initial theoretical [1, 2, 3, 4, 5, 6, 7, 8] and experimental [9] works, a first international meeting was devoted to the subject in St. Andrews (1965, [10]). Ten years later a second international meeting – in which the progress in the field of polarons

realized by 1972 was recorded – took place in Antwerpen [11]. Among the review papers and books covering the subject, we mention Refs. [12, 13, 14, 15].

Although the present course in Varenna 2005 mainly deals with “small” polarons (Holstein, Holstein-Hubbard), my contribution is devoted to “large” polarons. The reader is referred to most other papers in the present book for an overview of the properties of Holstein related polarons. In the present volume the contributions [16, 17, 18, 19] also deal with the Fröhlich polaron.

Let us recall the polaron concept for newcomers. A charge placed in a polarizable medium is screened. Dielectric theory describes the phenomenon by the induction of a polarization around the charge carrier. The induced polarization will follow the charge carrier when it is moving through the medium. The carrier together with the induced polarization is considered as one entity (see Fig.1). It was Pekar who came up with the term *polaron* [21]. The physical properties of a polaron differ from those of a band-carrier. A polaron is characterized by its *binding (or self-) energy* E_0 , an *effective mass* m^* and by its characteristic *response* to external electric and magnetic fields (e. g. dc mobility and optical absorption coefficient).

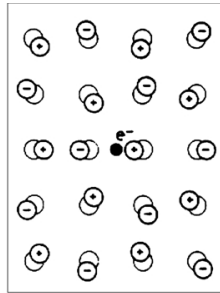


Fig. 1. – Artist view of a polaron. A conduction electron in an ionic crystal or a polar semiconductor repels the negative ions and attracts the positive ions. A self-induced potential arises, which acts back on the electron and modifies its physical properties. (From [20].)

If the spatial extension of a polaron is large compared to the lattice parameter of the solid, the latter can be treated as a polarizable continuum. This is the case of a *large, or continuum (Fröhlich)* polaron. When the self-induced polarization caused by an electron or hole becomes of the order of the lattice parameter, a *small (Holstein)* polaron can arise. As distinct from large polarons, small polarons are governed by short-range interactions.

1.1. The Fröhlich Hamiltonian. – Fröhlich proposed a model Hamiltonian for the “large” polaron through which its dynamics is treated quantum mechanically (“Fröhlich Hamiltonian”). The polarization, carried by the longitudinal optical (LO) phonons, is represented by a set of quantum oscillators with frequency ω_{LO} , the long-wavelength LO-phonon frequency, and the interaction between the charge and the polarization field

is linear in the field [6]:

$$(1) \quad H = \frac{\mathbf{p}^2}{2m_b} + \sum_{\mathbf{k}} \hbar\omega_{\text{LO}} a_{\mathbf{k}}^{\dagger} a_{\mathbf{k}} + \sum_{\mathbf{k}} (V_k a_{\mathbf{k}} e^{i\mathbf{k}\cdot\mathbf{r}} + V_k^* a_{\mathbf{k}}^{\dagger} e^{-i\mathbf{k}\cdot\mathbf{r}}),$$

where \mathbf{r} is the position coordinate operator of the electron with band mass m_b , \mathbf{p} is its canonically conjugate momentum operator; $a_{\mathbf{k}}^{\dagger}$ and $a_{\mathbf{k}}$ are the creation (and annihilation) operators for longitudinal optical phonons of wave vector \mathbf{k} and energy $\hbar\omega_{\text{LO}}$. The V_k are the Fourier components characterising the electron-phonon interaction

$$(2) \quad V_k = -i \frac{\hbar\omega_{\text{LO}}}{k} \left(\frac{4\pi\alpha}{V} \right)^{\frac{1}{2}} \left(\frac{\hbar}{2m_b\omega_{\text{LO}}} \right)^{\frac{1}{4}}.$$

The strength of the electron-phonon interaction is expressed by a dimensionless coupling constant α , which is defined as:

$$(3) \quad \alpha = \frac{e^2}{\hbar} \sqrt{\frac{m_b}{2\hbar\omega_{\text{LO}}}} \left(\frac{1}{\varepsilon_{\infty}} - \frac{1}{\varepsilon_0} \right).$$

In this definition, ε_{∞} and ε_0 are, respectively, the electronic and the static dielectric constant of the ionic crystal or polar semiconductor.

In Ref. [20]) the Fröhlich coupling constant is given for a few solids⁽¹⁾.

In deriving the form of V_k , expressions (2) and (3), it was assumed that (i) the spatial extension of the polaron is large compared to the lattice parameter of the solid (“continuum” approximation), (ii) spin and relativistic effects can be neglected, (iii) the band-electron has parabolic dispersion, (iv) in line with the first approximation it is also assumed that the LO-phonons of interest for the interaction, are the long-wavelength phonons with constant frequency ω_{LO} .

The model, represented by the Hamiltonian (1), (which up to now could not been solved exactly) has been the subject of extensive investigations, see, e. g., Refs. [3, 10, 12, 11, 22, 13, 14, 23]. In what follows the key approaches of the Fröhlich-polaron theory are briefly summarized with indication also of their relevance for the polaron problems in nanostructures.

2. – The Structure of the Polaron Excitation Spectrum and Optical Absorption by Polarons

2.1. Optical absorption at weak coupling. – At zero temperature and in the weak-coupling limit, the optical absorption is due to the elementary polaron scattering process, schematically shown in Fig. 2.

⁽¹⁾ In some cases, due to lack of reliable experimental data to determine the electron band mass, the values of α are not well established.

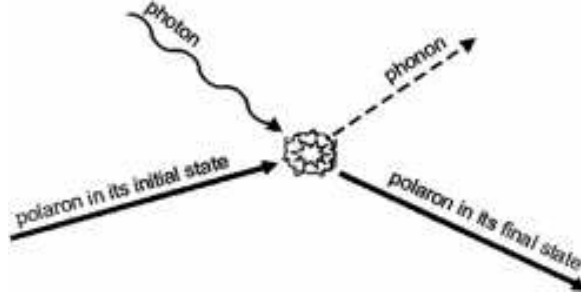


Fig. 2. – Elementary polaron scattering process describing the absorption of an incoming photon and the generation of an outgoing phonon.

In the weak-coupling limit ($\alpha \ll 1$) the polaron absorption coefficient was first studied by V. Gurevich, I. Lang and Yu. Firsov [24]. Their optical-absorption coefficient is equivalent to a particular approximation of the result of J. Tempere and J. T. Devreese (Ref. [25]), with the dynamic structure factor $S(\mathbf{k}, \Omega)$ corresponding to the Hartree-Fock approximation (see also [26], p. 585).

The result of Ref. [25] gives the Fröhlich polaron optical absorption coefficient for a many-polaron gas (in terms of the dynamic structure factor $S(\mathbf{k}, \Omega)$) exactly to order α . The real part of the optical conductivity of the N -polaron system for any N is obtained in Ref. [25] in an intuitively transparent form

$$(4) \quad \text{Re}[\sigma(\Omega)] = \frac{n}{\hbar\Omega^3} \frac{e^2}{m_b^2} \sum_{\mathbf{k}} k_x^2 |V_{\mathbf{k}}|^2 S(\mathbf{k}, \Omega - \omega_{LO}),$$

where $n = N/V$ is the density of charge carriers and k_x is the x -component of the wave vector (the electric field is along the x -axis). This approach to the many-polaron optical absorption allows one to include the many-body effects in terms of the dynamical structure factor

$$(5) \quad S(\mathbf{k}, \Omega) = \int_{-\infty}^{+\infty} \left\langle \varphi_{\text{el}} \left| \frac{1}{2} \sum_{j,\ell} e^{i\mathbf{k}\cdot(\mathbf{r}_j(t) - \mathbf{r}_\ell(0))} \right| \varphi_{\text{el}} \right\rangle e^{i\Omega t} dt$$

of the *electron (or hole) system*. Substituting Eq. (2) in Eq. (4), the following analytical

result was obtained in Ref. [25]⁽²⁾:

$$(6) \quad \text{Re}[\sigma(\Omega)] = ne^2 \frac{2\alpha}{3} \frac{1}{\sqrt{2\pi}\Omega^3} \int_0^{+\infty} dk k^2 S(k, \Omega - \omega_{\text{LO}}).$$

For $N = 1$, substituting a δ -function for the dynamical structure factor

$$S(\mathbf{k}, \Omega) \rightarrow \delta \left[\frac{\hbar k^2}{2m_b} - (\Omega - \omega_{\text{LO}}) \right]$$

in the general expression (4), the one-polaron limit Ref. [27] is retrieved. This one-polaron result is derived [27] by considering a process, in which the initial state consists of a photon of energy $\hbar\Omega$ and a polaron in its ground state, and the final state consists of an emitted LO phonon with energy $\hbar\omega_{\text{LO}}$ and the polaron, scattered into a state with momentum \mathbf{k} and kinetic energy $(\hbar k)^2/(2m_b) = \hbar(\Omega - \omega_{\text{LO}})$. The many-polaron result (4) is a generalization of the one-polaron picture. The contribution which corresponds to the scattering of a polaron into the momentum state \mathbf{k} and energy $\hbar(\Omega - \omega_{\text{LO}})$ is now weighed by the dynamical structure factor $S(\mathbf{k}, \Omega - \omega_{\text{LO}})$ of the electron (or hole) gas.

In the zero-temperature limit, within the weak coupling approximation, the real part of the polaron optical conductivity has the following analytic expression (see [27]) :

$$(7) \quad \text{Re} \sigma (\Omega) = \frac{\pi e^2}{2m^*} \delta (\Omega) + \frac{2e^2}{3m_b} \frac{\omega_{\text{LO}}^{3/2} \alpha}{\Omega^3} \sqrt{\Omega - \omega_{\text{LO}}} \Theta (\Omega - \omega_{\text{LO}}),$$

where

$$\Theta(\Omega - \omega_{\text{LO}}) = \begin{cases} 1 & \text{if } \Omega > \omega_{\text{LO}}, \\ 0 & \text{if } \Omega < \omega_{\text{LO}}. \end{cases}$$

The spectrum of the real part of the polaron optical conductivity (7) is represented in Fig. 3. The absorption coefficient for absorption of light with frequency Ω by a gas of free polarons for $\alpha \rightarrow 0$ takes the form

$$(8) \quad \Gamma_p(\Omega) = \frac{n_0}{\epsilon_0 c n} \frac{\pi e^2}{2m^*} \delta (\Omega) + \frac{1}{\epsilon_0 c n} \frac{2ne^2 \alpha \omega_{\text{LO}}^2}{3m_b \Omega^3} \sqrt{\frac{\Omega}{\omega_{\text{LO}}} - 1} \Theta (\Omega - \omega_{\text{LO}}),$$

where ϵ_0 is the dielectric permittivity of the vacuum, n is the refractive index of the medium, n_0 is the concentration of polarons. A simple derivation in Ref. [28] using a canonical transformation method gives the absorption coefficient of free polarons, which coincides with the second term in the result (8). A step function in (8) reflects the fact that at zero temperature the absorption of light accompanied by the emission of a phonon

⁽²⁾ A denominator of the prefactor in the Eq. (23) of Ref. [25] contain a misprint: there should be $\sqrt{2}$ instead of 2.

can occur (i) at $\Omega = 0$ and (ii) if the energy of the incident photon is larger than that of a phonon ($\Omega > \omega_{\text{LO}}$). The second term in the absorption coefficient (8) was obtained in Ref. [24] in the low-concentration region. In the weak-coupling limit, according to Eq. (8), the absorption spectrum consists of a central peak [$\propto \delta(\Omega)$] and a “one-phonon sideband”. At nonzero temperature, the absorption of a photon can be accompanied not only by emission, but also by absorption of one or more phonons.

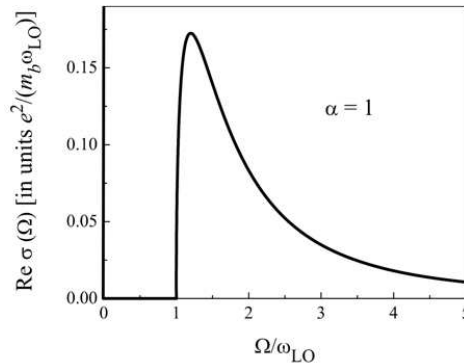


Fig. 3. – Polaron optical conductivity for $\alpha = 1$ in the weak-coupling approximation. (After [27], p. 92.) A δ -like central peak (at $\Omega = 0$) is schematically shown by a vertical line.

Experimentally, this one-phonon-sideband structure has been observed for free polarons e.g. in the infrared absorption spectra of CdO-films, see Fig. 4. In CdO, which is a weakly polar material with $\alpha \approx 0.74$, the polaron absorption band is observed in the spectral region between 6 and 20 μm (above the LO phonon frequency). The difference between theory and experiment in the wavelength region where polaron absorption dominates the spectrum is due to many-polaron effects.

2.2. Optical Absorption at Strong Coupling. – The problem of the structure of the large polaron excitation spectrum constituted a central question in the early stages of the development of polaron theory. The exactly solvable polaron model of Ref. [31] (see Appendix A) was used to demonstrate the existence of the so-called “relaxed excited states” of large polarons [32]. In Ref. [33], and after earlier intuitive analysis, this problem was studied using the classical equations of motion and Poisson-brackets. The insight gained as a result of those investigations concerning the structure of the excited polaron states, was subsequently used to develop a theory of the optical absorption spectra of polarons. The first work was limited to the strong coupling limit [34]. Ref. [34] is the first work that reveals the impact of the internal degrees of freedom of polarons on their optical properties.

The optical absorption of light by free Fröhlich polarons was treated in Ref. [34] using the polaron states obtained within the adiabatic strong-coupling approximation. It was argued in Ref. [34], that for sufficiently large α ($\alpha > 3$), the (first) relaxed excited state

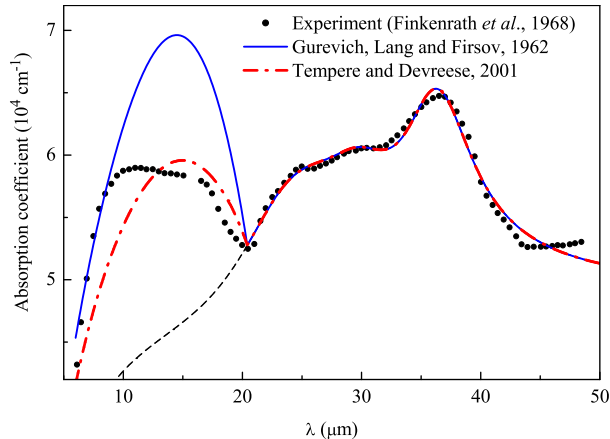


Fig. 4. – Optical absorption spectrum of a CdO-film with the carrier concentration $n = 5.9 \times 10^{19} \text{ cm}^{-3}$ at $T = 300 \text{ K}$. The experimental data (solid dots) of Ref. [29] are compared to different theoretical results: with (solid curve) and without (dashed line) the one-polaron contribution of Ref. [24] and for many polarons (dash-dotted curve) of Ref. [25]. The material parameters of CdO used for calculations: $\alpha = 0.74$ [29], $\omega_{\text{LO}} = 490 \text{ cm}^{-1}$ (from the experimental optical absorption spectrum, Fig. 2 of Ref. [29]), $m_b = 0.11m_e$ [30], $\varepsilon(0) = 21.9$, $\varepsilon(\infty) = 5.3$ [30].

(RES) of a polaron is a relatively stable state, which can participate in optical absorption transitions. This idea was necessary to understand the polaron optical absorption spectrum in the strong-coupling regime. The following scenario of a transition, which leads to a “zero-phonon” peak in the absorption by a strong-coupling polaron, can then be suggested. If the frequency of the incoming photon is equal to $\Omega_{\text{RES}} = 0.065\alpha^2\omega_{\text{LO}}$, the electron jumps from the ground state (which, at large coupling, is well-characterized by “s”-symmetry for the electron) to an excited state (“2p”), while the lattice polarization in the final state is adapted to the “2p” electronic state of the polaron. In Ref. [34] considering the decay of the RES with emission of one real phonon it is argued, that the “zero-phonon” peak can be described using the Wigner-Weisskopf formula valid when the linewidth of that peak is much smaller than $\hbar\omega_{\text{LO}}$.

For photon energies larger than $\Omega_{\text{RES}} + \omega_{\text{LO}}$, a transition of the polaron towards the first scattering state, belonging to the RES, becomes possible. The final state of the optical absorption process then consists of a polaron in its lowest RES plus a free phonon. A “one-phonon sideband” then appears in the polaron absorption spectrum. This process is called *one-phonon sideband absorption*. The one-, two-, ... K -, ... phonon sidebands of the zero-phonon peak give rise to a broad structure in the absorption spectrum. It turns out that the *first moment* of the phonon sidebands corresponds to the Franck-Condon (FC) frequency $\Omega_{\text{FC}} = 0.141\alpha^2\omega_{\text{LO}}$. To summarize, the polaron optical absorption spectrum at strong coupling is characterized by the following features (at $T = 0$):

- a) An intense absorption peak (“zero-phonon line”) appears, which corresponds to a transition from the ground state to the first RES at Ω_{RES} .
- b) For $\Omega > \Omega_{\text{RES}} + \omega_{\text{LO}}$, a phonon sideband structure arises. This sideband structure peaks around Ω_{FC} .

The qualitative behaviour predicted in Ref. [34], namely, an intense zero-phonon (RES) line with a broader sideband at the high-frequency side, was confirmed after an all-coupling expression for the polaron optical absorption coefficient had been studied [35].

2.3. Optical Absorption of Continuum Polarons at Arbitrary Coupling. – The polaron absorption coefficient $\Gamma(\Omega)$ of light with frequency Ω at arbitrary coupling was first derived by the present author and collaborators [35] (see also [36]). It was represented in the form

$$(9) \quad \Gamma(\Omega) = -\frac{1}{n\epsilon_0 c} \frac{e^2}{m_b} \frac{\text{Im} \Sigma(\Omega)}{[\Omega - \text{Re} \Sigma(\Omega)]^2 + [\text{Im} \Sigma(\Omega)]^2}.$$

This general expression was the starting point for a derivation of the theoretical optical absorption spectrum of a single Fröhlich polaron at *all electron-phonon coupling strengths* in Ref. [35]. $\Sigma(\Omega)$ is the so-called “memory function”, which contains the dynamics of the polaron and depends on Ω , α and temperature. The key contribution of the work in [35] was to introduce $\Gamma(\Omega)$ in the form (9) and to calculate $\text{Re} \Sigma(\Omega)$, which is essentially a (technically not trivial) Kramers–Kronig transform of the more simple function $\text{Im} \Sigma(\Omega)$. The function $\text{Im} \Sigma(\Omega)$ had been formally derived for the Feynman polaron [37] who studied the polaron mobility μ from the impedance function, i. e. the static limit

$$\mu^{-1} = \lim_{\Omega \rightarrow 0} \left(\frac{\text{Im} \Sigma(\Omega)}{\Omega} \right).$$

The nature of the polaron excitations was clearly revealed through this polaron optical absorption obtained in [35, 36]. It was demonstrated in [35] that the Franck-Condon states for Fröhlich polarons are nothing else but a superposition of phonon sidebands. It was also established in [35] that a relatively large value of the electron-phonon coupling strength ($\alpha > 5.9$) is needed to stabilise the relaxed excited state of the polaron. It was, further, revealed that at weaker coupling only “scattering states” of the polaron play a significant role in the optical absorption [35, 38].

In the weak coupling limit, the optical absorption spectrum (9) of the polaron is determined by the absorption of radiation energy, which is reemitted in the form of LO phonons. For $\alpha \gtrsim 5.9$, the polaron can undergo transitions toward a relatively stable RES (see Fig. 5). The RES peak in the optical absorption spectrum also has a phonon sideband-structure, whose average transition frequency can be related to a FC-type transition. Furthermore, at zero temperature, the optical absorption spectrum of one polaron exhibits also a zero-frequency “central peak” [$\propto \delta(\Omega)$]. For non-zero

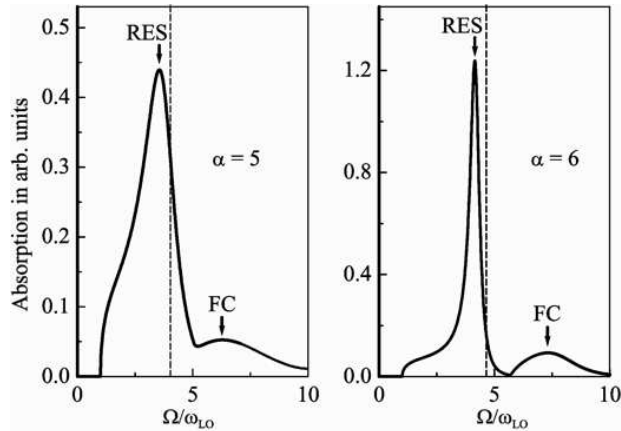


Fig. 5. – Optical absorption spectrum of a Fröhlich polaron for $\alpha = 5$ and $\alpha = 6$. The RES peak is very intense compared with the FC peak. The frequency $\Omega/\omega_{LO} = v$ is indicated by the dashed lines. The δ -like central peaks (at $\Omega = 0$) are schematically shown by vertical lines. (From Devreese *et al.* Ref. [35].)

temperature, this “central peak” smears out and gives rise to an “anomalous” Drude-type low-frequency component of the optical absorption spectrum.

For example, in Fig. 5 (from Ref. [35]), the main peak of the polaron optical absorption for $\alpha = 5$ at $\Omega = 3.51\omega_{LO}$ is interpreted as due to transitions to a RES. A “shoulder” at the low-frequency side of the main peak is attributed to one-phonon transitions to polaron-“scattering states”. The broad structure centered at about $\Omega = 6.3\omega_{LO}$ is interpreted as a FC band. As seen from Fig. 5, when increasing the electron-phonon coupling constant to $\alpha=6$, the RES peak at $\Omega = 4.3\omega_{LO}$ stabilizes. It is in Ref. [35] that the all-coupling optical absorption spectrum of a Fröhlich polaron, together with the role of RES-states, FC-states and scattering states, was first presented. Based on Ref. [35], it was argued that it is rather Holstein polarons that determine the optical properties of the charge carriers in oxides like SrTiO₃, BaTiO₃ [39], while large weak coupling polarons could be identified e. g. in CdO [40]. The Fröhlich coupling constants of polar semiconductors and ionic crystals are generally too small to allow for a static “RES”. In Ref. [41] the RES-peaks of Ref. [35] were involved to explain the optical absorption spectrum of Pr₂NiO_{4.22}. Further study of the spectra of [41] is called for. The RES-like resonances in $\Gamma(\Omega)$, Eq. (9), due to the zeros of $\Omega - \text{Re} \Sigma(\Omega)$, can effectively be displaced to smaller polaron coupling by applying an external magnetic field B , in which case the contribution for what is formally a “RES-type resonance becomes $\Omega - \omega_c - \text{Re} \Sigma(\Omega) = 0$ ($\omega_c = eB/m_b c$ is the cyclotron frequency). Resonances in the magnetoabsorption governed by this contribution have been widely observed and analysed [42] to [54] (see also Subsection 3.2 below).

Recent interesting numerical calculations of the optical conductivity for the Fröhlich

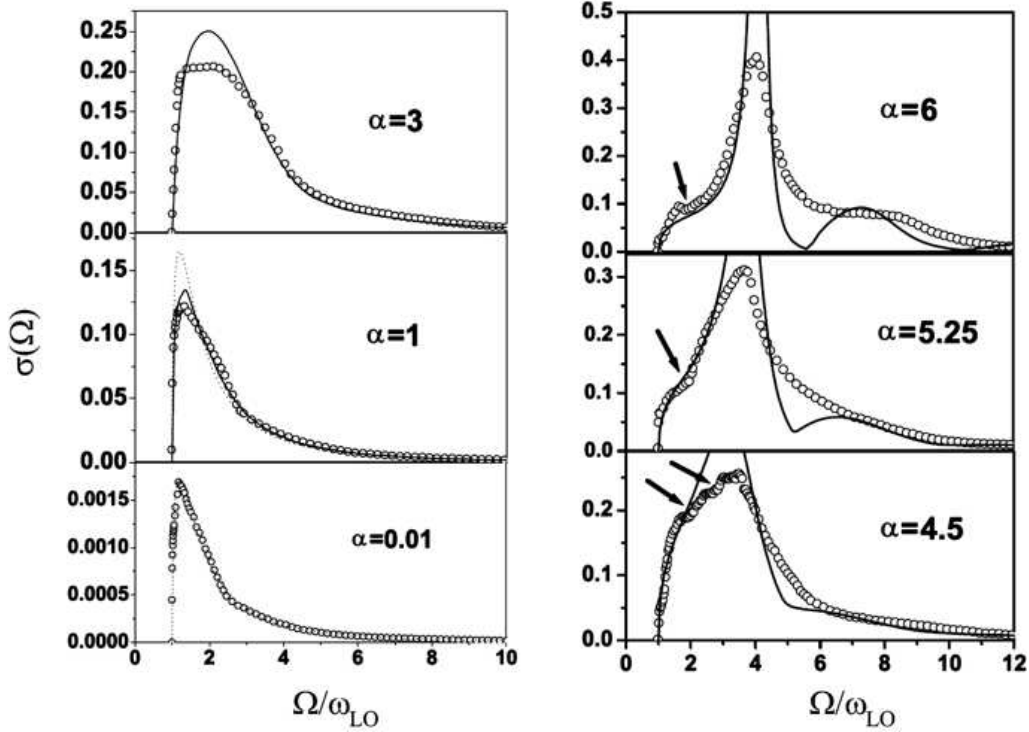


Fig. 6. – *Left-hand panel*: Monte Carlo optical conductivity spectra of one Fröhlich polaron for the weak-coupling regime (open circles) compared to the second-order perturbation theory (dotted lines) for $\alpha = 0.01$ and $\alpha = 1$ and to the analytical DSG calculations [35] (solid lines). *Right-hand panel*: Monte Carlo optical conductivity spectra for the intermediate coupling regime (open circles) compared to the analytical DSG approach [35] (solid lines). Arrows point to the two- and three-phonon thresholds. (From Ref. [55].)

polaron performed within the Diagrammatic Quantum Monte Carlo (DQMC) method [55], see Fig. 6, fully confirm the essential analytical results derived in Ref. [35] for $\alpha \lesssim 3$. In the intermediate coupling regime $3 < \alpha < 6$, the low-energy behavior and the position of the RES-peak in the optical conductivity spectrum of Ref. [55] follow closely the prediction of Ref. [35]. There are some minor qualitative differences between the two approaches in the intermediate coupling regime: in Ref. [55], the dominant (“RES”) peak is less intense in the Monte-Carlo numerical simulations and the second (“FC”) peak develops less prominently. The following qualitative differences exist between the two approaches in the strong coupling regime: in Ref. [55], the dominant peak broadens and the second peak does not develop, giving instead rise to a flat shoulder in the optical conductivity spectrum at $\alpha = 6$. These qualitative differences from the optical absorption spectrum of Ref. [35] can be tentatively attributed to the optical processes

TABLE I. – Polaron parameters M_0, M_1, \tilde{M}_0 obtained from the diagrammatic Monte Carlo results

α	$M_0^{(\text{MC})}$	$m^{*(\text{MC})}$	$\tilde{M}_0^{(\text{MC})}$	$M_1^{(\text{MC})}/\alpha$	$E_0^{(\text{MC})}$
0.01	0.00249	1.0017	1.5706	0.634	-0.010
1	0.24179	1.1865	1.5657	0.65789	-1.013
3	0.67743	1.8467	1.5280	0.73123	-3.18
4.5	0.97540	2.8742	1.5219	0.862	-4.97
5.25	1.0904	3.8148	1.5022	0.90181	-5.68
6	1.1994	5.3708	1.4919	0.98248	-6.79
6.5	1.30	6.4989	1.5417	1.1356	-7.44
7	1.3558	9.7158	1.5175	1.2163	-8.31
8	1.4195	19.991	1.4981	1.3774	-9.85

with participation of two [56] or more phonons. The above differences can arise also due to the fact that, starting from the Feynman polaron model, one-phonon processes are assigned more oscillator strength and the RES of [35] therefore tends to be more stable as compared to the Monte-Carlo result. The comparison of the analytical and numerical results for the optical absorption of the Fröhlich polarons shown in Fig. 6 deserves further study. An independent numerical simulation is called for.

2.4. Sum Rules for the Optical Conductivity Spectra. – In this section the sum rules for the optical conductivity spectra of Fröhlich polarons obtained within the DSG approach [35] are compared with those found from the DQMC results [55]. The values of the polaron effective mass for the Monte Carlo approach are taken from Ref. [23]. In Tables I and II, I show the polaron ground-state E_0 and the following parameters calculated using the optical conductivity spectra:

$$(10) \quad M_0 \equiv \int_1^{\omega_{\max}} \text{Re } \sigma(\omega) d\omega,$$

$$(11) \quad M_1 \equiv \int_1^{\omega_{\max}} \omega \text{Re } \sigma(\omega) d\omega,$$

where ω_{\max} is the upper value of the frequency available from Ref. [55],

$$(12) \quad \tilde{M}_0 \equiv \frac{\pi}{2m^*} + \int_1^{\omega_{\max}} \text{Re } \sigma(\omega) d\omega,$$

where m^* is the polaron mass, the optical conductivity is calculated in units $n_0 e^2 / (m_b \omega_{\text{LO}})$, m^* is measured in units of the band mass m_b , and the frequency is measured in units of ω_{LO} . The values of ω_{\max} are: $\omega_{\max} = 10$ for $\alpha = 0.01, 1$ and 3 , $\omega_{\max} = 12$ for $\alpha = 4.5, 5.25$ and 6 , $\omega_{\max} = 18$ for $\alpha = 6.5, 7$ and 8 .

The parameters corresponding to the Monte Carlo calculation are obtained using the numerical data kindly provided to the author by A. Mishchenko [57]. The optical

TABLE II. – Polaron parameters M_0, M_1, \tilde{M}_0 obtained within the path-integral approach

α	$M_0^{(\text{DSG})}$	$m^{*(\text{Feynman})}$	$\tilde{M}_0^{(\text{DSG})}$	$M_1^{(\text{DSG})}/\alpha$	$E_0^{(\text{Feynman})}$
0.01	0.00248	1.0017	1.5706	0.633	-0.010
1	0.24318	1.1957	1.5569	0.65468	-1.0130
3	0.69696	1.8912	1.5275	0.71572	-3.1333
4.5	1.0162	3.1202	1.5196	0.83184	-4.8394
5.25	1.1504	4.3969	1.5077	0.88595	-5.7482
6	1.2608	6.8367	1.4906	0.95384	-6.7108
6.5	1.3657	9.7449	1.5269	1.1192	-7.3920
7	1.4278	14.395	1.5369	1.2170	-8.1127
8	1.4741	31.569	1.5239	1.4340	-9.6953

conductivity obtained within the path-integral approach of Ref. [35] exactly satisfies the sum rule [58]

$$(13) \quad \frac{\pi}{2m^*} + \int_1^\infty \text{Re } \sigma(\omega) d\omega = \frac{\pi}{2}.$$

Since the optical conductivity obtained from the Monte Carlo results [55] is known only within a limited interval of frequencies $1 < \omega < \omega_{\text{max}}$, we calculate the integral in Eq. (12) for the DSG-approach [35] over the same frequency interval as for the Monte Carlo results [55].

The comparison of the resulting zero frequency moments $\tilde{M}_0^{(\text{MC})}$ and $\tilde{M}_0^{(\text{DSG})}$ with each other and with the value $\pi/2 = 1.5707963\dots$ corresponding to the right-hand-side of the sum rule (13) shows that the difference $|\tilde{M}_0^{(\text{MC})} - \tilde{M}_0^{(\text{DSG})}|$ on the interval $\alpha \leq 8$ is smaller than the absolute value of the contribution of the “tail” of the optical conductivity for $\omega > \omega_{\text{max}}$ to the integral in the sum rule (13):

$$(14) \quad \int_{\omega_{\text{max}}}^\infty \text{Re } \sigma^{(\text{DSG})}(\omega) d\omega \equiv \frac{\pi}{2} - \tilde{M}_0^{(\text{DSG})}.$$

Within the accuracy determined by the neglect of the “tail” of the part of the spectrum for $\omega > \omega_{\text{max}}$, the contribution to the integral in the sum rule (13) for the optical conductivity obtained from the Monte Carlo results [55] *agrees well* with that for the optical conductivity found within the path-integral approach of Ref. [35]. Hence, the conclusion follows that *the optical conductivity obtained from the Monte Carlo results [55] satisfies the sum rule (13) within the aforementioned accuracy.*

We analyze also the fulfillment of the “LSD” polaron ground-state theorem introduced in [59]

$$(15) \quad E_0(\alpha) - E_0(0) = -\frac{3}{\pi} \int_0^\alpha \frac{d\alpha'}{\alpha'} \int_0^\infty \omega \text{Re } \sigma(\omega, \alpha') d\omega$$

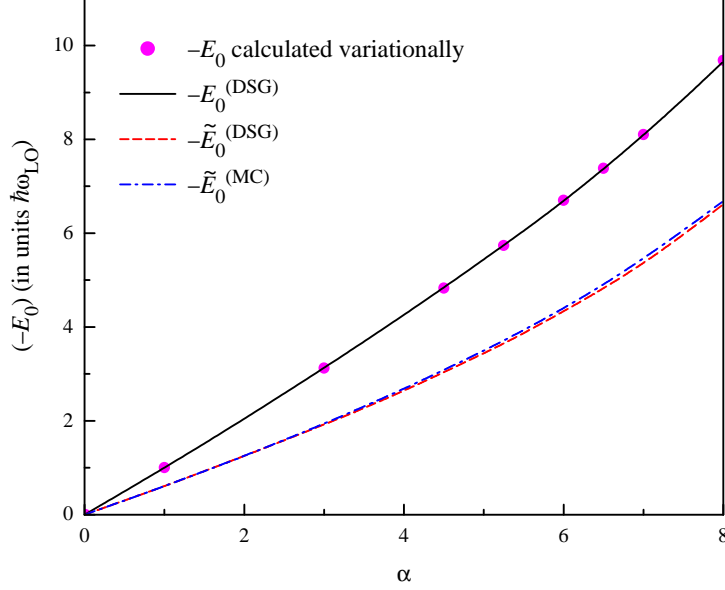


Fig. 7. – Test of the ground-state theorem for a Fröhlich polaron from Ref. [59] using different optical conductivity spectra, DSG from Ref. [35] and MC from Ref. [55]. The notations are explained in the text.

using the first-frequency moments $M_1^{(\text{MC})}$ and $M_1^{(\text{DSG})}$. The results of this comparison are presented in Fig. 7. The dots indicate the polaron ground-state energy calculated using the Feynman variational principle. The solid curve is the value of $E_0(\alpha)$ calculated numerically using the optical conductivity spectra and the ground-state theorem with the DSG optical conductivity [35] for a polaron,

$$(16) \quad E_0^{(\text{DSG})}(\alpha) \equiv -\frac{3}{\pi} \int_0^\alpha \frac{d\alpha'}{\alpha'} \int_0^\infty \omega \text{Re} \sigma^{(\text{DSG})}(\omega, \alpha') d\omega.$$

The dashed and the dot-dashed curves are the values obtained using $M_1^{(\text{DSG})}(\alpha)$ and $M_1^{(\text{MC})}(\alpha)$, respectively:

$$(17) \quad \tilde{E}_0(\alpha) \equiv -\frac{3}{\pi} \int_0^\alpha \frac{d\alpha'}{\alpha'} \int_0^{\omega_{\text{max}}} \omega \text{Re} \sigma(\omega, \alpha') d\omega = -\frac{3}{\pi} \int_0^\alpha d\alpha' \frac{M_1(\alpha')}{\alpha'}.$$

As seen from the figure, $E_0^{(\text{DSG})}(\alpha)$ to a high degree of accuracy coincides with the variational polaron ground-state energy. Both $\tilde{E}_0^{(\text{DSG})}(\alpha)$ and $\tilde{E}_0^{(\text{MC})}(\alpha)$ differ from $E_0^{(\text{DSG})}(\alpha)$ due to the integration over the same limited frequency interval. However, $\tilde{E}_0^{(\text{DSG})}(\alpha)$ and $\tilde{E}_0^{(\text{MC})}(\alpha)$ are very close to each other. Herefrom, the conclusion follows that for integrals over the finite frequency region characteristic for the polaron optical

absorption (i. e., omitting the “tails”), the function $\tilde{E}_0^{(\text{MC})}(\alpha)$ reproduces very well the function $\tilde{E}_0^{(\text{DSG})}(\alpha)$.

From the comparison of $\tilde{E}_0^{(\text{DSG})}(\alpha)$ with $\tilde{E}_0^{(\text{MC})}(\alpha)$ it follows that the contribution to the integral in (17) with the limited frequency region, which approximates the integral in the right-hand side of the “LSD” ground state theorem (15), for the optical conductivity obtained from the Monte Carlo results [55] *agrees with a high accuracy* with the corresponding contribution to the integral in (17) for the optical conductivity found within the path-integral approach of Ref. [35]. Because for the path-integral result, the integral $\tilde{E}_0^{(\text{DSG})}(\alpha)$ noticeably differs from the available integral $E_0^{(\text{DSG})}(\alpha)$, a comparison between the Feynman polaron ground state energy E_0 and the integral $\tilde{E}_0^{(\text{DSG})}(\alpha)$ is not representative. Similarly, a comparison between the polaron ground state energy obtained from the Monte Carlo results and the integral $\tilde{E}_0^{(\text{MC})}(\alpha)$ would require to overcome the present limitation for the available optical conductivity spectrum [55].

In conclusion, the Monte Carlo optical conductivity spectrum for higher frequencies than ω_{max} of [55] is needed in order to check the fulfillment of the sum rules (13) and (15) with a higher accuracy.

3. – Scaling Relations for Fröhlich Polarons

Several scaling relations connect the polaron self-energy, the effective mass, the impedance Z and the polaron mobility μ in 2D to their counterpart in 3D. Those relations were introduced in Ref. [60] (Peeters and Devreese), they are satisfied at the level of the Feynman polaron model and are listed here:

$$(18a) \quad E_{2\text{D}}(\alpha) = \frac{2}{3} E_{3\text{D}} \left(\frac{3\pi}{4} \alpha \right),$$

$$(18b) \quad \frac{m_{2\text{D}}^*(\alpha)}{m_{2\text{D}}} = \frac{m_{3\text{D}}^* \left(\frac{3}{4} \alpha \right)}{m_{3\text{D}}},$$

$$(18c) \quad Z_{2\text{D}}(\alpha, \Omega) = Z_{3\text{D}} \left(\frac{3\pi}{4} \alpha, \Omega \right),$$

$$(18d) \quad \mu_{2\text{D}}(\alpha) = \mu_{3\text{D}} \left(\frac{3\pi}{4} \alpha \right).$$

In Eq. (18b), $m_{2\text{D}}^*$ ($m_{3\text{D}}^*$) and $m_{2\text{D}}$ ($m_{3\text{D}}$) are, respectively, the polaron and the electron-band masses in 2D (3D). Expressions (18) provide a straightforward link between polaron characteristics in 3D with those in 2D. The scaling relations imply that polaron effects may be observable in 2 dimensions at substantially lower electron-phonon coupling than in 3 dimensions. Against this background, an extensive analysis of polaronic phenomena was undertaken for GaAs heterostructures, quantum wells, superlattices, 2D oxide-structures, shallow donors (“bound polarons”) and also for quantum dots, see e. g. Refs. [61] to [64] and the reviews [13, 20].

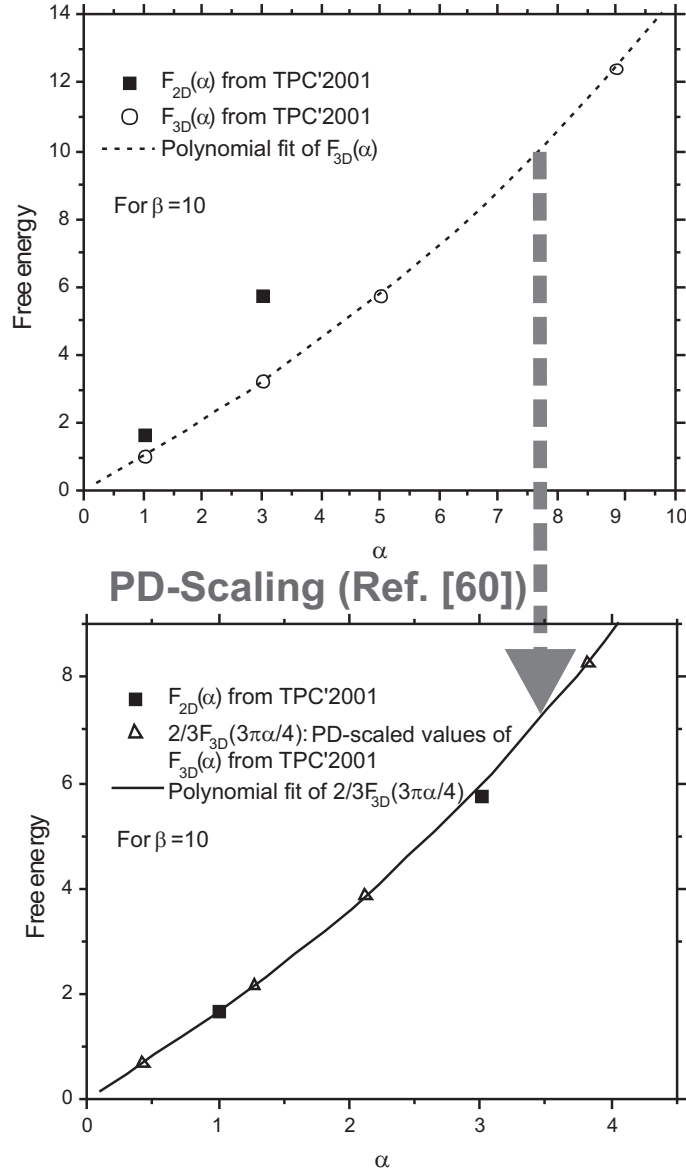


Fig. 8. – *Upper panel*: Polaron free energy in 3D (squares) and 2D (open circles) obtained by TPC'2001 [65] for $\beta = 10$. The data for $F_{3D}(\alpha)$ are interpolated using a polynomial fit to the available four points (dotted line). *Lower panel*: Demonstration of the PD-scaling cf. Peeters-Devreese [60]: the polaron free energy in 2D obtained by TPC'2001 [65] for $\beta = 10$ (squares) is very close to the **PD-scaled** according to Peeters-Devreese [60] values of the polaron free energy in 3D from TPC'2001 for $\beta = 10$ (open triangles). The data for $\frac{2}{3}F_{3D}(\frac{3\pi\alpha}{4})$ are interpolated using a polynomial fit to the available four points (solid line).

31. *Check of the scaling relation for the path integral Monte Carlo results for the polaron free energy.* – The fulfillment of the PD-scaling relation [60] is now checked for the path integral Monte Carlo results [65] for the polaron free energy. The path integral Monte Carlo results of Ref. [65] for the polaron free energy in 3D and in 2D were given for a few values of temperature and for some selected values of α . For a check of the scaling relation, the values of the polaron free energy at $\beta = 10$ are taken from Ref. [65] in 3D (Table I of Ref. [65], for four values of α) and in 2D (Table II of Ref. [65], for two values of α) and plotted in Fig. 8, upper panel, with squares and open circles, correspondingly. In Fig. 8, lower panel, the available data for the free energy from Ref [65] are plotted in the following form *inspired by the l.h.s. and the r.h.s parts of Eq. (18a)*: $F_{2D}(\alpha)$ (squares) and $\frac{2}{3}F_{3D}(\frac{3\pi\alpha}{4})$ (open triangles). As follows from the figure, *the path integral Monte Carlo results for the polaron free energy in 2D and 3D very closely follow the PD-scaling relation of the form given by Eq. (18a)*:

$$(19) \quad F_{2D}(\alpha) \equiv \frac{2}{3}F_{3D}\left(\frac{3\pi\alpha}{4}\right).$$

32. *Magnetoabsorption spectra of polarons.* – The results on the polaron optical absorption [35, 27] paved the way for an all-coupling path-integral based theory of magneto-optical absorption by polarons (see Ref. [42], F. Peeters and J. T. Devreese). This work was i. a. motivated by the insight that magnetic fields can stabilise the relaxed excited polaron states, so that information on the nature of relaxed excited states might be gained from the cyclotron resonance of polarons. A quantitative interpretation of the high-precision cyclotron resonance experiment on AgBr and AgCl in a range of magnetic fields up to 15 T [44] by the theory of Ref. [42] provided one of the most convincing and clearest demonstrations of polaron features in solids. For a review of the subsequent developments in the field of polaron cyclotron resonance, the reader is referred to Refs. [49, 66, 52, 53, 67, 13, 20] and references therein. The energy spectra of such polaronic systems as shallow donors (“bound polarons”), e. g., the D_0 and D^- centres, constitute the most complete and detailed polaron spectroscopy realised in the literature, see for example Fig. 9.

4. – Many-Polaron Systems

41. *Ground State and the Optical Absorption Spectra of Many-Polaron Systems.* – The earliest studies on many polarons concerned their role in heavily doped polar semiconductors [69, 70, 71]. The possibility that polarons and bipolarons play a role in high- T_c superconductors has renewed interest in the physical properties of many-polaron systems and, in particular, in their optical properties. Theoretical treatments have been extended from one-polaron to many-polaron systems both of Fröhlich polarons (see, for example, [72, 73, 74, 20, 75, 76, 77, 78]) and of Holstein polarons (see, e. g., [79, 80, 81]).

For the weak-coupling regime, which is realized in most polar semiconductors, the ground-state energy of a gas of interacting large polarons was derived in Ref. [73] by

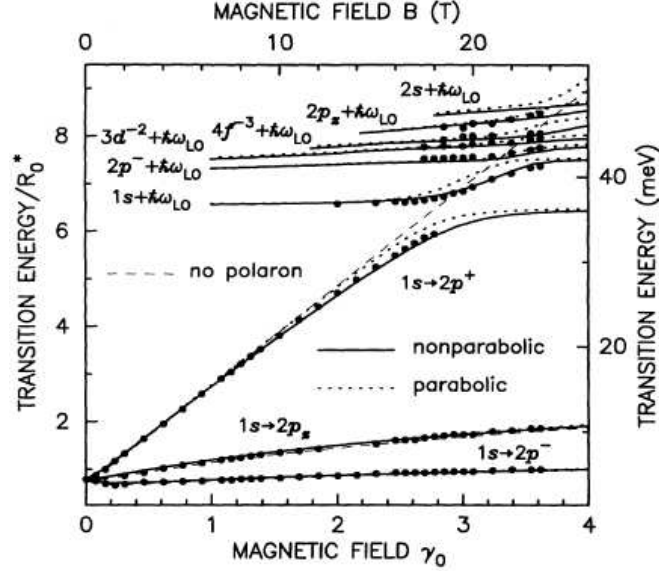


Fig. 9. – The $1s \rightarrow 2p^\pm, 2p_z$ transition energies as a function of a magnetic field for a donor in GaAs. We compare our theoretical results for the following cases: (a) without the effect of polaron and band nonparabolicity (thin dashed curves); (b) with polaron correction (dotted curves); (c) including the effects of polaron and band nonparabolicity (solid curves) to the experimental data of Ref. [68] (solid dots). (From Ref. [66].)

introducing a variational wave function:

$$(20) \quad |\psi_{\text{LDB}}\rangle = U |\phi\rangle |\varphi_{\text{el}}\rangle,$$

where $|\varphi_{\text{el}}\rangle$ represents the ground-state many-body wave function for the electron (or hole) system, $|\phi\rangle$ is the phonon vacuum and U is a many-body unitary operator that determines a canonical transformation for a fermion gas interacting with a boson field:

$$(21) \quad U = \exp \left\{ \sum_{j=1}^N \sum_{\mathbf{k}} (f_{\mathbf{k}} a_{\mathbf{k}} e^{i\mathbf{k}\cdot\mathbf{r}_j} - f_{\mathbf{k}}^* a_{\mathbf{k}}^+ e^{-i\mathbf{k}\cdot\mathbf{r}_j}) \right\},$$

where \mathbf{r}_j represent the position vectors of the N constituent electrons (or holes); $a_{\mathbf{k}}^+, a_{\mathbf{k}}$ denote the creation and annihilation operators for LO phonons with wave vector \mathbf{k} . The $f_{\mathbf{k}}$ were determined variationally [73]. It may be emphasized that the expression (21) constitutes – especially in its implementation – a nontrivial extension of the one-particle approximation to a many-body system. An advantage of the many-polaron canonical transformations introduced in Ref. [73] for the calculation of the ground state energy of

a polaron gas is that, to order α , the many-body effects are entirely contained in the static structure factor of the electron (or hole) system, which appears in the analytical expression for the energy. The minimum of the total ground-state energy per particle as a function of the electron density for a polaron gas is shown [73] to lie at lower value of the density than that for the electron gas.

In Ref. [25], the optical absorption coefficient of an interacting many-polaron gas has been derived starting from the many-polaron canonical transformations and the variational many-polaron wave function introduced in Ref. [73]. The real part of the optical conductivity of the many-polaron system to order α is obtained in terms of the dynamical structure factor in Ref. [25] in the form (4), which has been discussed in the Subsection 2.1. The experimental peaks in the mid-infrared optical absorption spectra of (Fig. 10) and manganites (Fig. 11) have been interpreted within this theory, using (4). The experimental optical absorption spectrum (up to 3000 cm^{-1}) of $\text{Nd}_2\text{CuO}_{2-\delta}$

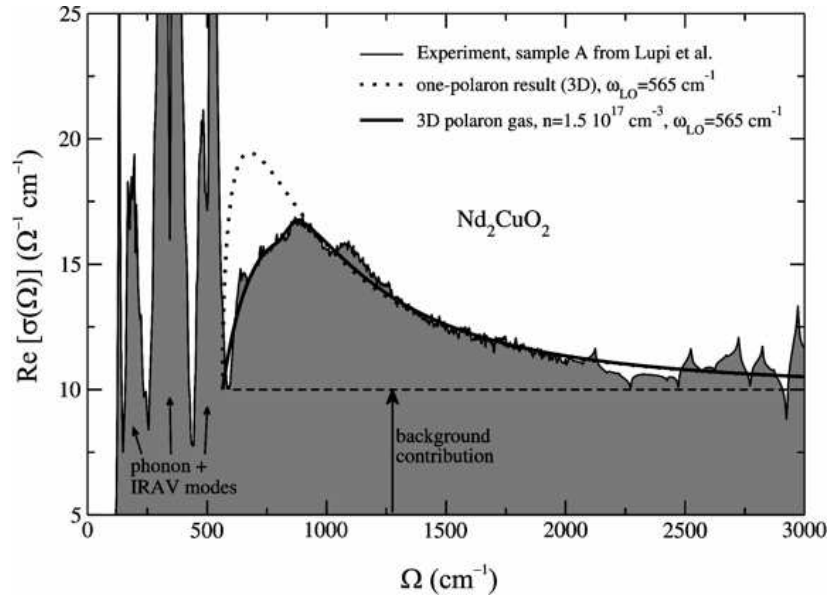


Fig. 10. – The infrared absorption of $\text{Nd}_2\text{CuO}_{2-\delta}$ ($\delta < 0.004$) is shown as a function of frequency, up to 3000 cm^{-1} . The experimental results of Calvani and co-workers [82] is represented by the thin black curve and by the shaded area. The so-called ‘d-band’ rises in intensity around 600 cm^{-1} and increases in intensity up to a maximum around 1000 cm^{-1} . The dotted curve shows the single polaron result. The full black curve represents the theoretical results obtained in the present work for the interacting many-polaron gas with $n_0 = 1.5 \times 10^{17} \text{ cm}^{-3}$, $\alpha = 2.1$ and $m_b = 0.5 m_e$. (Recently, a numerical inaccuracy was identified in the fitting procedure, concerning the strength of the plasmon branch, so that the parameter values given above may not be the optimal parameter values, see Ref. [83].) (From Ref. [25].)

($\delta < 0.004$), obtained by P. Calvani and co-workers [82], is shown in Fig. 10 (shaded area)

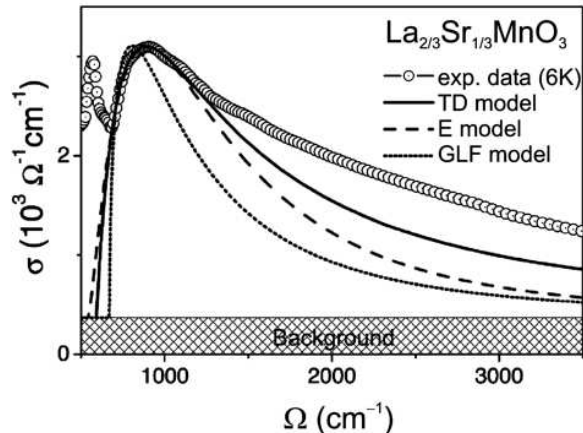


Fig. 11. – Comparison of the measured mid-infrared optical conductivity in $\text{La}_{2/3}\text{Sr}_{1/3}\text{MnO}_3$ at $T = 6$ K to that given by several model calculations for $m = 3m_e$, α of the order of 1 and $n_0 = 6 \times 10^{21} \text{ cm}^{-3}$. The one-polaron approximations [the weak-coupling approach by V. L. Gurevich, I. G. Lang, and Yu. A. Firsov [24] (GLF model) and the phenomenological approach by D. Emin [84] (E model)] lead to narrower polaron peaks than a peak with maximum at $\omega \sim 900 \text{ cm}^{-1}$ given by the many-polaron treatment by J. Tempere and J. T. Devreese (TD model) of Ref. [25]. (After Ch. Hartinger *et al.*, Ref. [85].)

together with the theoretical curve obtained by the method of Ref. [25] (full, bold curve) and, for reference, with the one-polaron optical absorption result (dotted curve). At lower frequencies ($600\text{--}1000 \text{ cm}^{-1}$) a marked difference between the single polaron optical absorption and the many-polaron result is manifest. The experimental *d*-band can be clearly identified, rising in intensity at about 600 cm^{-1} , peaking around 1000 cm^{-1} , and then decreasing in intensity above that frequency. At a density of $n_0 = 1.5 \times 10^{17} \text{ cm}^{-3}$, we found compelling agreement between our theoretical predictions and the experimental curve. The authors of Ref. [85] interpret their data on $\text{La}_{2/3}\text{Sr}_{1/3}\text{MnO}_3$ with Eq. (4) [25], adapted for an on-site Hubbard interaction.

The optical conductivity of a many-polaron gas was further investigated, by Iadonisi and associates, e. g. in Ref. [86] within the memory-function approach [35] by calculating the correction to the dielectric function of the electron gas, due to the electron-phonon interaction with variational parameters of a single-polaron Feynman model. A suppression of the optical absorption from the one-polaron optical absorption of Ref. [35] with increasing density shown in Fig. 12 is expected because of the screening of the Fröhlich interaction with increasing polaron density.

Recently, dynamical exchange effects were found to lead to noticeable corrections to the random-phase approximation results for the ground state energy, the effective mass, and the optical conductivity of a two-dimensional many-polaron gas in Refs. [87, 83].

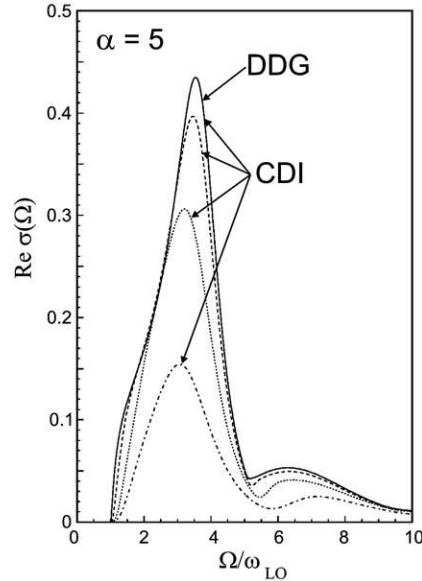


Fig. 12. – Optical conductivity of a polaron gas at $T = 0$ as a function of the frequency as calculated in Ref. [86] (CDI) for different values of the electron density: $n_0 = 1.4 \times 10^{-5}$ (solid curve), $n_0 = 1.4 \times 10^{-4}$ (dashed curve), $n_0 = 1.4 \times 10^{-3}$ (dotted curve), and $n_0 = 1.4 \times 10^{-2}$ (dotted-dashed curve). The electron density is measured per R_p^3 , where R_p is the Fröhlich polaron radius. The value of $\varepsilon_0/\varepsilon_\infty$ is 3.4. The solid curve practically coincides with the known optical conductivity of a single polaron [35] (DDG). (After Ref. [86].)

4.2. Many-Polaron Cyclotron Resonance in Quantum Wells. – In GaAs/AlAs quantum wells with high electron density, anticrossing of the cyclotron-resonance spectra has been observed near the GaAs transverse optical (TO) phonon frequency ω_{T1} rather than near the GaAs LO-phonon frequency ω_{L1} [88]. This anticrossing near ω_{T1} was explained in the framework of the polaron theory in Refs. [89, 91] (Fig. 13). This effect is in contrast with the cyclotron resonance of a low-density polaron gas in a quantum well, where anticrossing occurs near the LO-phonon frequency. The appearance of the anticrossing frequency close to ω_{T1} instead of ω_{L1} is due to the screening of the electron-phonon interaction by the plasma oscillations. The theory takes into account the magnetoplasmon-phonon mixing and the electron-phonon interaction with all the phonon modes specific for the quantum well. A discussion on alternative explanations of the data of Ref. [88] is still going on [90, 91, 92].

4.3. Interacting Polarons in a Quantum Dot. – A system of N electrons (or holes) with mutual Coulomb repulsion and interacting with the bulk phonons is analysed in Refs. [93, 64]. It has been shown [94] that the path-integral approach to the many-body problem for a fixed number of identical particles can be formulated as a Feynman-Kac functional

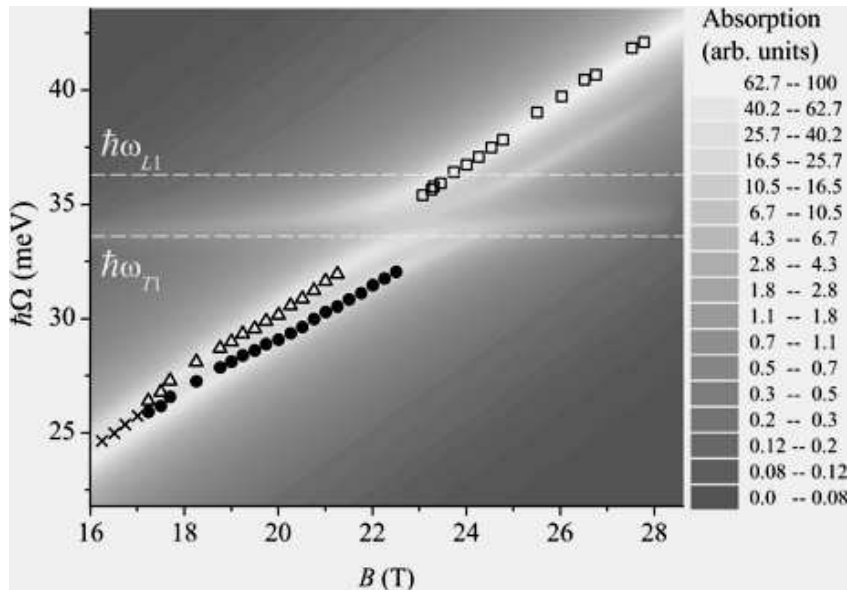


Fig. 13. – Density map of the magnetoabsorption spectrum for a 10-nm GaAs/AlAs quantum well as calculated in Ref. [89]. Peak positions of the experimental spectra are taken from Fig. 3 of Ref. [88]. Crosses indicate the CR peak positions for $B \leq 17$ T. Above 17 T, the CR line splits into two components represented by triangles and by filled dots. This splitting occurs due to the fact, that the electron Landau levels in a non-parabolic conduction band are non-equidistant. The higher- and lower-energy components correspond to the transitions between the Landau levels ($0 \rightarrow 1$) and ($1 \rightarrow 2$), respectively. A single CR line shown by squares is observed above 23 T. Dashed lines show LO- and TO-phonon energies in GaAs. (After Ref. [89].)

on a state space for N indistinguishable particles. The resulting variational inequality for identical particles [95] formally has the same structure as the Jensen-Feynman variational principle [96]. A model system consisting of N electrons and N_f fictitious particles in a harmonic confinement potential with elastic interparticle interactions is studied in Refs. [93, 64]. The Lagrangian of this model system is symmetric with respect to electron permutations. The parameters of the model system are found from the variational principle [95] and used for the calculation of the ground-state energy and the optical conductivity of the N -polaron system in a quantum dot [93, 64].

The polaron contribution to the ground-state energy of the N -polaron system in a quantum dot per particle calculated within our variational path-integral treatment for different N [97] is compared with the respective quantity for a polaron gas in bulk, found in Ref. [99] within an intermediate-coupling approach and in Ref. [100], using a variational approach developed first in Ref. [73]. Our all-coupling variational method [97] provides somewhat lower values for the polaron contribution than those obtained in Refs. [99, 100] and the trends predicted in those references are confirmed.

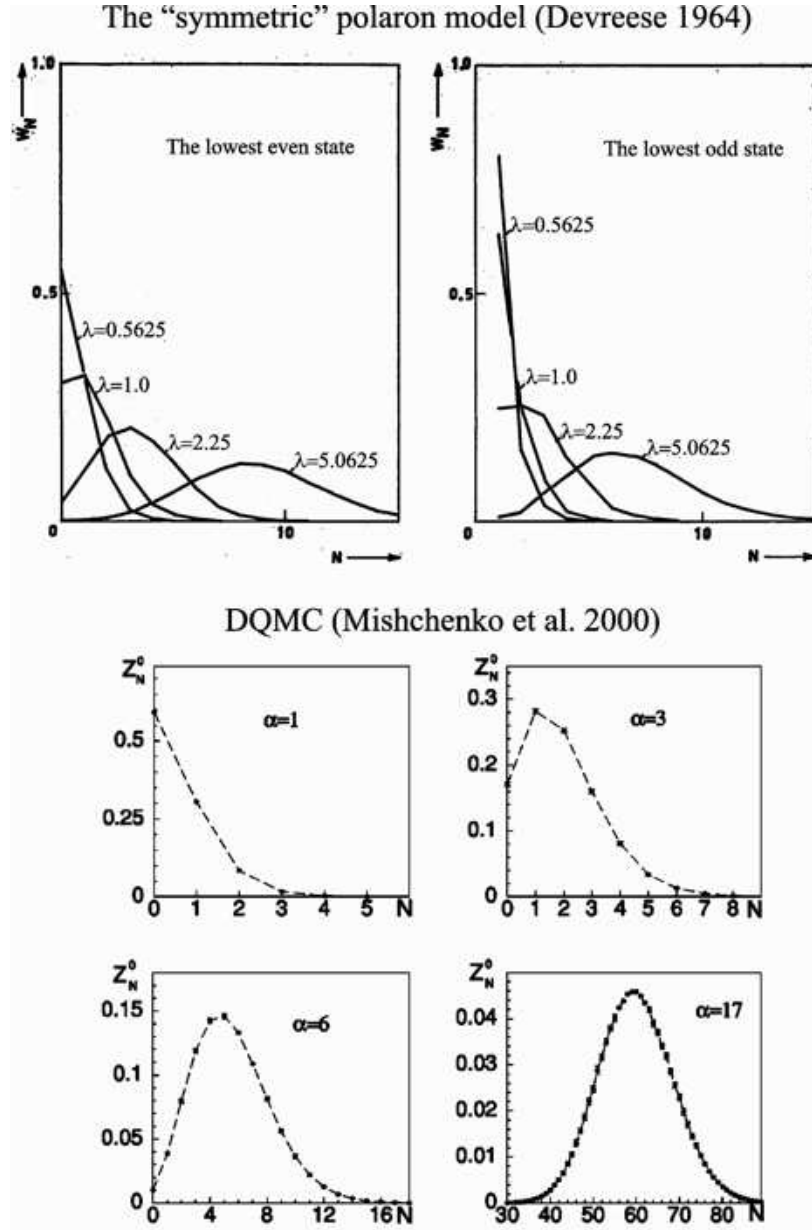


Fig. 14. – *Upper panel*: The phonon distribution functions W_N in the “symmetric” polaron model for various values of the effective coupling constant λ at $\varkappa = 1, \mathbf{P} = 0$ (from [31], Fig. 23). *Lower panel*: Distribution of multiphonon states in the polaron cloud within DQMC method for various values of α (from [23], Fig. 7).

APPENDIX A.

On the Contributions of the N -phonon States to the Polaron Ground State

In Ref. [31], the present author introduced and analysed an exactly solvable (“symmetric”) 1D-polaron model. The further study of this model was performed in Refs. [32, 101]. This model can be used as a tool for the evaluation of the accuracy of the standard polaron theories [102, 103, 104].

The model consists of an electron interacting with two oscillators possessing opposite wave vectors: \mathbf{k} and $-\mathbf{k}$. The parity operator, which changes $a_{\mathbf{k}}$ and $a_{-\mathbf{k}}$ (and also $a_{\mathbf{k}}^\dagger$ and $a_{-\mathbf{k}}^\dagger$), commutes with the Hamiltonian of the system. Hence, the polaron states are classified into even and odd states with eigenvalues of the parity operator $+1$ and -1 , respectively. For the lowest even and odd states, the phonon distribution functions W_N are plotted in Fig. 14, upper panel, for some values of the effective coupling constant λ of this “symmetric” model. The value of the parameter $\varkappa = \sqrt{(\hbar k)^2 / m_b \hbar \omega_{LO}}$ for these graphs was taken to be 1, while the total polaron momentum $\mathbf{P} = 0$. In the weak-coupling case ($\lambda \approx 0.6$) W_N is a decaying function of N . When increasing λ , W_N acquires a maximum, e. g. at $N = 8$ for the lowest even state at $\lambda = 5.0625$. The phonon distribution function W_N has the same character for the lowest even and the lowest odd states at all values of the number of the virtual phonons in the ground state (as distinct from the higher states). This led to the conclusion that the lowest odd state is an internal excited state of the polaron.

In Ref. [23], the structure of the Fröhlich polaron cloud was investigated using the DQMC method. Contributions of N -phonon states to the polaron ground state were calculated as a function of N for a few values of the coupling constant α , see Fig. 14, lower panel. The evolution from the weak-coupling case ($\alpha = 1$) into the strong-coupling regime ($\alpha = 17$) was studied. Comparison of the lower panel to the upper panel in Fig. 14 shows that the evolution of the shape and the scale of the distribution of the N -phonon states with increasing α as derived for a Fröhlich polaron within DQMC method [23] is *in notable agreement* with the results obtained within the “symmetric” 1D polaron model [31, 32, 101].

* * *

I thank V. M. Fomin for discussions of the present paper and S. N. Klimin for interactions on some aspects of this work. The present work has been supported by the GOA BOF UA 2000, IUAP, FWO-V projects G.0306.00, G.0274.01N, G.0435.03, the WOG WO.035.04N (Belgium), the European Commission GROWTH Programme, NANOMAT project, contract No. G5RD-CT-2001-00545 and the European Commission SANDIE Network of Excellence, contract No. NMP4-CT-2004-500101.

REFERENCES

- [1] LANDAU L. D., *Phys. Z. Sowjetunion*, **3** (1933) 664.
- [2] LANDAU L. D. and PEKAR S. I., *Zh. Eksp. i Teor. Fiz.*, **18** (1948) 419.

- [3] PEKAR S. I., *Issledovanija po Ekelektronnoj Teorii Kristallov* (Gostekhizdat, Moskva) 1951 [German translation: *Untersuchungen über die Elektronentheorie der Kristalle* (Akademie Verlag, Berlin) 1951].
- [4] BOGOLUBOV, N. N., *Ukr. Matem. Zh.*, **2** (1950) 3.
- [5] BOGOLUBOV N. N. and TYABLIKOV S. V., *Zh. Eksp. i Teor. Fiz.*, **19** (1949) 256.
- [6] FRÖHLICH H., *Adv. Phys.*, **3** (1954) 325.
- [7] LEE T. D., LOW F. E. and PINES D., *Phys. Rev.*, **90** (1953) 297
- [8] FEYNMAN, R. P., *Phys. Rev.*, **97** (1955) 660.
- [9] BROWN F. C., (1963), in Ref. [10], pp. 323 - 355.
- [10] *Polarons and Excitons*, edited by KUPER G. C. and WHITFIELD G. D. (Oliver and Boyd, Edinburgh) 1963.
- [11] *Polarons in Ionic Crystals and Polar Semiconductors*, edited by DEVREESE J. T. (North-Holland, Amsterdam) 1972.
- [12] APPEL J., in *Solid State Physics*, edited by SEITZ J., TURNBULL J. and EHRENREICH J. (Academic Press, New York) 1968, vol. 21, pp. 193-391.
- [13] DEVREESE J. T., in *Encyclopedia of Applied Physics*, edited by TRIGG G. L. (VCH, Weinheim) 1996, vol 14, pp. 383-413.
- [14] ALEXANDROV A. S. and N. MOTT, *Polarons and Bipolarons* (World Scientific, Singapore) 1996.
- [15] CALVANI P., *Optical Properties of Polarons* (Editrice Compositori, Bologna) 2001.
- [16] CALVANI P., in *the present book*.
- [17] CATAUDELLA V., in *the present book*.
- [18] PERRONI C. A., in *the present book*.
- [19] MISHCHENKO A. S., in *the present book*.
- [20] DEVREESE J. T., in *Lectures on the Physics of Highly Correlated Electron Systems VII*, edited by AVELLA A. and MANCINI F. (AIP, Melville) 2003, pp. 3-56.
- [21] PEKAR S. I., *Zhurn. Exper. Teor. Fiz.*, **16** (1946) 341.
- [22] MITRA T. K., CHATTERJEE A. and MUKHOPADHYAY S., *Phys. Rep.*, **153** (1987) 91.
- [23] MISHCHENKO A. S., PROKOF'EV N. V. SAKAMOTO A. and SVISTUNOV B. V., *Phys. Rev. B*, **62** (2000) 6317.
- [24] GUREVICH V. L., LANG I. G., and FIRSOV YU. A., *Fiz. Tverd. Tela*, **4** (1962) 1252 [English translation: *Sov. Phys. — Solid St.*, **4** (1962) 918].
- [25] TEMPERE J. and DEVREESE J. T., *Phys. Rev. B*, **64** (2001) 104504.
- [26] MAHAN G. D., *Many-Particle Physics* (Kluwer/Plenum, New York) 2000.
- [27] DEVREESE J. T., in *Polarons in Ionic Crystals and Polar Semiconductors* (North-Holland, Amsterdam) 1972, pp. 83–159.
- [28] DEVREESE J. HUYBRECHTS W. and LEMMENS W., *Phys. Stat. Sol. (b)*, **48** (1971) 77.
- [29] FINKENRATH W., UHLE W. and WAIDELICH W., *Solid State Commun.*, **7** (1969) 11.
- [30] *Landolt-Börnstein Numerical Data and Functional Relationships in Science and Technology, New Series*, editor in chief HELLWEGE K.-H. (Springer, New York) 1982, Group III, Vol. 17, Subvolume b, pp. 161-165.
- [31] DEVREESE J. T., *Contribution to the polaron theory*, Ph.D. Thesis (unpublished), KU Leuven, 1964.
- [32] DEVREESE J. T. and EVRARD R., *Phys. Letters*, **11** (1964) 278.
- [33] EVRARD R., *Phys. Letters*, **14** (1965) 295.
- [34] KARTHEUSER E., EVRARD E., and DEVREESE J., *Phys. Rev. Lett.*, **22** (1969) 94.
- [35] DEVREESE J. T., DE SITTER J. and GOOVAERTS M., *Phys. Rev. B*, **5** (1972) 2367.
- [36] PEETERS F. M. and DEVREESE J. T., *Phys. Rev. B*, **28** (1983) 6051.
- [37] FEYNMAN R. P., HELLWARTH R. W., IDDIGS C. K., and PLATZMAN P. M., *Phys. Rev. B*, **127** (1962) 1004 1962.

- [38] DEVREESE J., DE SITTER J. and GOOVAERTS M., *Solid State Commun.*, **9** (1971) 1383.
- [39] HUYBRECHTS W. and DEVREESE J., *Solid State Commun.*, **17** (1975) 401.
- [40] DEVREESE J., HUYBRECHTS W. and LEMMENS L., *Phys. Stat. Sol. (b)*, **48** (1971) 77.
- [41] EAGLES D. M., LOBO R. P. S. M. and GERVAIS F., *Phys. Rev. B*, **52** (1995) 6440.
- [42] PEETERS F. M. and DEVREESE J. T., *Phys. Rev. B*, **34** (1986) 7246.
- [43] HOPKINS M.A., NICHOLAS R.J., PFEFFER P., ZAWADZKI W., GAUTHIER D., PORTAL J.C., and DiFORTE-POISSON M.A., *Semicond. Sci. Technol.*, **2** (1987) 568.
- [44] HODBY J.W., RUSSELL G.P., PEETERS F.M., DEVREESE J.T. and LARSEN D.M., *Phys. Rev. Lett.*, **58** (1987) 1471.
- [45] LANGERAK C.J.G.M., SINGLETON J., VAN DER WEL P.J., PERENBOOM J.A.A.J., BARNES D.J., NICHOLAS R.J., HOPKINS M.A. and FOXON C.T.B., *Phys. Rev. B*, **38** (1988) 13133.
- [46] NAJDA S.P., YOKOI H., TAKEYAMA S., MIURA N., PFEFFER P., and ZAWADZKI W., *Phys. Rev. B*, **40** (1989) 6189.
- [47] BARNES D.J., NICHOLAS R.J., PEETERS F.M., WU X.-G., DEVREESE J.T., SINGLETON J., LANGERAK C.J.G.M., HARRIS J.J. and FOXON C.T., *Phys. Rev. Lett.* **66** 1991 794.
- [48] KOBORI H., OHYAMA T. and OTSUKA E., *Solid State Commun.*, **84** (1992) 383.
- [49] PEETERS F.M., WU X.-G., DEVREESE J.T., LANGERAK C.J.G.M., SINGLETON J., BARNES D.J. and NICHOLAS R.J., *Phys. Rev. B*, **45** (1992) 4296.
- [50] NICHOLAS R.J., WATTS M., HOWELL D.F., PEETERS F.M., WU X.-G., DEVREESE J.T., VAN BOCKSTAL L., HERLACH F., LANGERAK C.J.G.M., SINGLETON J. and CHEVY A., *Phys. Rev. B*, **45** (1992) 12144.
- [51] VAUGHAN T.A., NICHOLAS R.J., LANGERAK C.J.G.M., MURDIN B.N., PIDGEON C.R., MASON N.J. and WALKER P.J., *Phys. Rev. B*, **53** (1996) 16481.
- [52] GRYNBERG M., HUANT S., MARTINEZ G., KOSSUT J., WOJTOWICZ T, KARCZEWSKI G., SHI J.M., PEETERS F.M. and DEVREESE J.T, *Phys. Rev. B*, **54** (1996) 1467.
- [53] WANG Y.-J., NICKEL H.A., MCCOMBE B.D., PEETERS F.M., SHI J.M., HAI G.Q., WU X.-G., EUSTIS T.J. and SCHAFF W., *Phys. Rev. Lett.*, **79** (1997) 3226.
- [54] MIURA N., NOJIRI H., PFEFFER P. and ZAWADZKI W., *Phys. Rev. B*, **55** (1997) 13598.
- [55] MISHCHENKO A. S., NAGAOSA N., PROKOF'EV N. V., SAKAMOTO A. and SVISTUNOV B. V., *Phys. Rev. Lett.*, **91** (2003) 236401.
- [56] GOOVAERTS M. J., DE SITTER J. and DEVREESE J. T., *Phys. Rev. B*, **7** 1973 2639.
- [57] MISHCHENKO A. S., *private communication*, () .
- [58] DEVREESE J. T., LEMMENS L. and VAN ROYEN J., *Phys. Rev. B*, **15** (1977) 1212.
- [59] LEMMENS L. F., DE SITTER J. and DEVREESE J. T., *Phys. Rev. B*, **8** (1973) 2717.
- [60] PEETERS F. M. and DEVREESE J. T., *Phys. Rev. B*, **36** (1987) 4442.
- [61] *The Physics of the Two-Dimensional Electron Gas*, edited by DEVREESE J. T. and PEETERS F. M., ASI Series, volume B 157 (Plenum, New York) 1987.
- [62] AUSTIN I. G. and MOTT N. F., *Advances in Physics*, **50** (2001) 757.
- [63] ALEXANDROV A. S. *Theory of Superconductivity. From Weak to Strong Coupling* (IOP Publishing, Bristol) 2003.
- [64] KLIMIN S. N., FOMIN V. M., BROSENS F. and DEVREESE J. T., *Phys. Rev. B*, **69** (2004) 235324.
- [65] TITANTAH J. T., PIERLEONI C., and CIUCHI C., *Phys. Rev. Lett.*, **87** (2001) 206406.
- [66] SHI J. M., PEETERS F. M. and DEVREESE J. T., *Phys. Rev. B*, **48** (1993) 5202.
- [67] PEETERS F.M., in *High Magnetic Fields: Science and Technology*, edited by HERLACH F. and MIURA N. (World Scientific, Singapore) 2003, vol. 2, p. 23-45.
- [68] CHENG J.-P., MCCOMBE B. D., SHI J. M., PEETERS F. M. and DEVREESE J. T., *Phys. Rev. B*, **48** (1993) 7910.
- [69] MAHAN G. D., (1972), in Ref. [11], pp. 553 - 657.
- [70] SERNELIUS BO E., *Phys. Rev. B*, **36** (1987) 4878.

- [71] SHERMAN E. YA., *Phys. Rev. B*, **67** (2003) 014304.
- [72] MAHAN G. D. and DUKE C. B., *Phys. Rev.*, **149** (1966) 705.
- [73] LEMMENS L. F. DEVREESE J. T. and BROSENS F., *Phys. Stat. Sol. (b)*, **82** (1977) 439.
- [74] FRATINI P. and QUÉMERAS P., *Eur. Phys. J. B*, **14** (2000) 99.
- [75] BASSANI F. G., CATAUDELLA V., CHIOFALO M. L., DE FILIPPIS G., IADONISI G. and PERRONI C. A., *Phys. Stat. Sol. (b)*, **(237)** 2003 173.
- [76] FRATINI S. and QUÉMERAS P., *European Phys. J. B*, **29** (2002) 41.
- [77] PERRONI C. A., IADONISI G. and MUKHOMOROV V. K., *European Phys. J. B*, **41** (2004) 163.
- [78] IADONISI G., MUKHOMOROV V. K., CANTELE G. and NINNO D., *Phys. Rev. B*, **72** (2005) 094305.
- [79] BERGER E., VALÁSEK P. and VON DER LINDEN W., *Phys. Rev. B*, **52** (1955) 4806.
- [80] FRATINI S., DE PASQUALE F. and CIUCHI S., *Phys. Rev. B*, **63** (2001) 153101.
- [81] TAKADA Y. and CHATTERJEE A., *Phys. Rev. B*, **67** (2003) 081102(R).
- [82] LUPI S., MASELLI P., CAPIZZI M., CALVANI P., GIURA P. and ROY P., *Phys. Rev. Lett.*, **83** (1999) 4852.
- [83] HAMEEUW K.J., TEMPERE J., BROSENS F. and DEVREESE J.T., *Eur. Phys. J. B*, **37** (2004) 447.
- [84] EMIN D., *Phys. Rev. B*, **48** (1993) 13691.
- [85] HARTINGER CH., MAYR F., DEISENHOFER J., LOIDL A., and KOPP T., *Phys. Rev. B*, **69** (2004) 100403(R).
- [86] CATAUDELLA V., DE FILIPPIS G. and IADONISI G., *Eur. Phys. J. B*, **12** (1999) 17.
- [87] HAMEEUW K.J., BROSENS F. and DEVREESE J.T., *Eur. Phys. J. B*, **35** (2003) 93. *Phys. Rev. Lett.*, **58** (1987) 1471.
- [88] POULTER A. J. L., ZEMAN J., MAUDE D. K., POTEMSKI M., MARTINEZ G., RIEDEL A., HEY R., and FRIEDLAND K. J., *Phys. Rev. Lett.*, **86** (2001) 336.
- [89] KLIMIN S. N. and DEVREESE J. T., *Phys. Rev. B*, **68** (2003) 245303.
- [90] FAUGERAS C., MARTINEZ G., RIEDEL A., HEY R., FRIEDLAND K. J. and BYCHKOV YU., *Phys. Rev. Lett.*, **92** (2004) 107403.
- [91] KLIMIN S. N. and DEVREESE J. T., *Phys. Rev. Lett.*, **94** (2005) 239701.
- [92] FAUGERAS C., MARTINEZ G. and BYCHKOV YU., *Phys. Rev. Lett.*, **94** (2005) 239702.
- [93] DEVREESE J. T., KLIMIN S. N., FOMIN V. M. and BROSENS F., *Solid State Communications*, **114** (2000) 305.
- [94] LEMMENS L. F., BROSENS F. and DEVREESE J. T., *Phys. Rev. E*, **53** (1996) 4467.
- [95] DEVREESE J. T., in *Fluctuating Paths and Fields* edited by JANKE W., PELSTER A., SCHMIDT H.-J. and BACHMANN M. (World Scientific, Singapore), 2001, pp. 283-299.
- [96] FEYNMAN R. P., *Statistical Mechanics* (Benjamin, Massachusetts) 1972.
- [97] BROSENS F., KLIMIN S. N. and DEVREESE J. T., *to be published*, () .
- [98] TARUCHA S., AUSTING D. G., HONDA T., VAN DER HAGE R. J. and KOUWENHOVEN L. P., *Phys. Rev. Lett.*, **77** (1996) 3613.
- [99] DE FILIPPIS G., CATAUDELLA V. and IADONISI G., *Eur. Phys. J. B*, **8** (1999) 339.
- [100] DA COSTA W.B. and STUART N., *Phys. Rev. B*, **47** (1993) 6356.
- [101] DEVREESE J. T. and EVRARD R., *Proceedings of the British Ceramic Society*, **10** (1968) 151. Reprinted in *Path Integrals and Their Applications in Quantum, Statistical, and Solid State Physics*, edited by PAPADOPOULOS G. J. and DEVREESE J. T. (*NATO ASI Series B, Physics*, vol. 34) (Plenum, New York) 1977, pp. 344-357.
- [102] DEVREESE J. T. and EVRARD R., *Phys. Stat. Sol.*, **3** (1963) 2133.
- [103] DEVREESE J. T. and EVRARD R., *Phys. Stat. Sol.*, **9** (1965) 403.
- [104] DEVREESE J. T. and EVRARD R., *Phys. Letters*, **23** (1966) 196.